Polymer Chemistry

Accepted Manuscript

This is an *Accepted Manuscript*, which has been through the Royal Society of Chemistry peer review process and has been accepted for publication.

Accepted Manuscripts are published online shortly after acceptance, before technical editing, formatting and proof reading. Using this free service, authors can make their results available to the community, in citable form, before we publish the edited article. We will replace this *Accepted Manuscript* with the edited and formatted *Advance Article* as soon as it is available.

You can find more information about *Accepted Manuscripts* in the Information for Authors.

Please note that technical editing may introduce minor changes to the text and/or graphics, which may alter content. The journal's standard Terms & Conditions and the Ethical guidelines still apply. In no event shall the Royal Society of Chemistry be held responsible for any errors or omissions in this *Accepted Manuscript* or any consequences arising from the use of any information it contains.

ROYAL SOCIETY OF CHEMISTRY

www.rsc.org/polymers

Polymer Chemistry

RSCPublishing

ARTICLE

Impact of thienothiophene isomeric structures on the optoelectronic properties and photovoltaic performance in quinoxaline based donor-acceptor copolymers

Cite this: DOI: 10.1039/xoxxoooooox

Received ooth January 2012,
Accepted ooth January 2012

DOI: 10.1039/xoxxoooooox

www.rsc.org/

Ranbir Singh,[1] Georgia Pagona,[2,3] Vasilis G. Gregoriou,[2,3] Nikos Tagmatarchis,[3] Dimosthenis Toliopoulos,[1] Yang Han,[4] Zhuping Fei,[4] Athanasios Katsouras,[5] Apostolos Avgeropoulos,[5] Thomas D. Anthopoulos,[6] Martin Heeney,[4] Panagiotis E. Keivanidis,[7*] and Christos L. Chochos[2,5*]

The influence of the monomer's isomeric structures on the optical, electrochemical, charge transporting properties and photovoltaic performance of donor-acceptor (D-A) conjugated polymers is demonstrated for the first time by studying two D-A copolymers consisting of the bis(3-octyloxy)phenyl)quinoxaline as the electron deficient unit and the two isomeric structures of thienothiophene (thieno[3,2-*b*]thiophene and thieno[2,3-*b*]thiophene) as the electron rich units. The drastic effect of incorporating two different isomeric structures on the polymer backbone of these copolymers, manifests on changes observed in their optical, electrochemical and charge transporting properties. On the contrary, the overall photovoltaic performance of the copolymers is similar, but distinct differences on the device photocurrents occur. These differences on the device photocurrents were attributed to morphology variations rather than the balanced mobility ratio. For further developments in the field, the isomeric structures of different functional monomers should be considered in the designing of new materials with even superior performance.

1. Introduction

Polymeric semiconductors are materials where unique optical and electronic properties often originate from a tailored chemical structure.[1,2] During the past few decades a vast number of conjugated polymers have been developed and various chemical modifications are used to engineer and optimize the physical and optoelectronic properties that suit their specific purpose.[3,4] Two major methodologies are employed to fine tune the band gap and energy level alignment of conjugated polymers. One methodology relies on the donor-acceptor (D-A) approach and the other on the stabilization of the quinoid structure.[5]

Common monomer units function as electron donors include the bridged biphenylenes and bithiophenes, benzodithiophenes, thienothiophenes, benzotrithiophenes, naphthodithiophenes, etc.[6] On the other hand, electron acceptor units used to construct D-A polymers possess at least one or more strong electron withdrawing groups, like an imine nitrogen, or carboxyl unit. Typical electron deficient moieties are thiazole-, thiadiazole-, pyrazine- and annulated amide or imide- based derivatives.[7] Other parameters influencing the optoelectronic properties of polymeric semiconductors are the electron donating or accepting side groups, while side chains with different nature regarding length and branching and their positioning onto the polymeric backbone are mostly employed to influence the regioregularity, through solid state packing, and solubility.[8]

Recently, many issues related to how the relative strength, the placement and the ratio of the donor and acceptor moieties in the backbone of D-A conjugated polymers influence the positioning of the HOMO, LUMO levels and as a consequence the electrochemical band gap, as well as the optical band gap have been addressed.[9,10] However the critical issue of the effect of the monomer's isomeric structures on the optoelectronic properties and performance in different applications of various polymeric semiconductors has been poorly addressed. The most common electron rich building blocks, 4*H*-cyclopenta[2,1-*b*:3,4-*b*′]dithiophene along with the silicon and germanium bridged analogues, benzo[1,2-*b*:4,5-*b*′]dithiophene and naphtha[2,3-*b*:6,7-*b*′]dithiophene (Figure S1 in Supporting Information (SI)) are extensively used as the electron rich moieties for the development of new D-A conjugated polymers.[11] However, the majority of the different isomeric structures of these monomers has been rarely employed (Figure S1 in SI).

Very few examples that have been reported studying the influence of the different isomeric structures on the optical,

structural and transporting properties in fused polythiophene derivatives and all these examples are related to organic field effect transistors (OFETs). *Müllen et al.* compared five polythiophene derivatives containing different benzodithiophene isomers in OFETs.[12] It has been shown that the optical gap increased with increasing curvature of the polymers. The more highly curved polymers possess reduced order in the film, whereas the less curved ones have too low solubility for processing. *McCulloch, Heeney et al.* have developed a series of quaterthiophene derivatives based on the two isomeric structures of thienothiophene (thieno[2,3-*b*]thiophene and thieno[3,2-*b*]thiophene) and various alkyl side chains and examined their structural conformation along with the OFET performance.[13] A maximum mobility of 0.15 $cm^2 V^{-1}s^{-1}$ was found for T23T quaterthiophene with decyl side chains. On the other hand, T32T quaterthiophene derivatives exhibit higher structural order combined with the increased backbone rigidity. This is reflected in mobilities as high as 0.72 $cm^2 V^{-1}s^{-1}$ for the tetradecyl-substituted T32T quaterthiophene copolymer. *Takimiya et al.* has studied in details the electronic properties of the four isomeric structures of fused naphthodithiophenes, as well as their polymeric analogues, and evaluated their performances in organic and polymeric FETs.[14] The angular-naphthodithiophene-based polymers displayed lower HOMO levels and larger band gaps than their linear counterparts. The polymers with angular naphthodithiophenes, on the other hand, provided the highly ordered structures with a very close π-stacking distance of 3.6 Å, whereas those with linear naphthodithiophenes had a very weak or no π-stacking order. As a result, the polymer bearing naphtho[1,2-*b*:5,6-*b'*]dithiophene, an angular-shaped naphthodithiophene, exhibited the highest mobility of ~0.8 $cm^2 V^{-1}s^{-1}$ among the four polymers with isomeric naphthodithiophenes.[14]

Hitherto, no studies have been made on the effect of the monomers of isomeric structure in donor-acceptor copolymers in the organic photovoltaic performance. For this reason we present here the design rules for and to demonstrate the synthesis of two donor – acceptor conjugated polymers consisting of quinoxaline as the electron withdrawing unit and the two isomeric forms of thienothiophene (T23T and T32T) as the electron rich units (Scheme 1). Our results highlight the influence of the isomeric structures of the thiophene-fused aromatic compounds on the optoelectronic properties and photovoltaic performance of the corresponding donor-acceptor polymeric semiconductors. The obtained electronic properties and photovoltaic performances for the two thienothiophene-*alt*-quinoxaline copolymers are compared and discussed using TQ1 polymer as a reference (inset in Scheme 1). TQ1 namely poly(2,3-bis-(3-octyloxyphenyl)quinoxaline-5,8-dyl-alt-thiophene-2,5-diyl) is the unfused thiophene analogue of T32TQ and T23TQ which can be easily synthesized,[15] has a relatively high bandgap (1.7 eV) ideal for tandem solar cells and exhibits high PCE up to 7.0%.[16] Very recently, the influence of the quinoxaline's side-chain geometry on the ability of the TQ1 to order as well as on the backbone conformation was presented in detail.[17]

Scheme 1.

2. Results and Discussion

2.1. Synthesis

The D-A copolymers of Scheme 1 were synthesized by Stille aromatic cross-coupling polymerization utilizing tris(dibenzylideneacetone)dipalladium(0) (Pd_2dba_3) in 1% per mole and tri(*o*-tolyl)phosphine ($P(o\text{-tol})_3$), 2% per mole, as the catalytic system in toluene solution between the 5,8-dibromo-2,3-bis(3-(octyloxy)phenyl)quinoxaline (1) and the distannyl derivatives bearing either thiophene (2), thieno[3,2-*b*]thiophene; [T32T] (3) and thieno[2,3-*b*]thiophene; [T23T] (4). In this series of oligothiophene copolymers, the thiophene, T32T and T23T units constitute the electron rich units while the quinoxaline unit is the electron deficient moiety. The polymerization reactions were performed at 110 °C under argon atmosphere for 48 h. After purification using Soxhlet extraction, the chloroform-soluble fractions of the TQ1, T32TQ and T23TQ copolymers exhibit molecular weights of M_n = 33000 g/mol (PDI =2.6), 20000 g/mol (PDI=2.0) and 20000 g/mol (PDI=2.0), respectively as measured by gel permeation chromatography (GPC) based on monodisperse polystyrene standards. Copolymers T32TQ and T23TQ provide the same molecular weights (M_n) despite the fact of the two different thienothiophene isomeric forms. The thermal stability of the copolymers characterized by thermogravimetric analysis (TGA) in nitrogen atmosphere (Figure S2 in SI). While TQ1 and T32TQ are stable up to 450 °C, T23TQ exhibit a 5% weight-loss at this temperature. After 450 °C all the copolymers are degraded.

Table 1.

2.2. Optical and Electrochemical Properties

The absorption spectra of co-polymers T23TQ, T32TQ and TQ1 in chloroform solution and as thin films are presented in Figure 1, and the corresponding optoelectronic properties are summarized in Table 1. The incorporation of the two different isomeric forms of thienothiophene has a noticeable impact on the optical properties of the T23TQ and T32TQ, as shown in the absorption spectra of Figure 2. While T23TQ exhibits a pronounced double absorption peaks at 342 nm, 600 nm in solution, qualitatively similar to TQ1, T32TQ display three absorption bands at 353 nm, 616 nm and 656 nm (Figure 1a). The absorption peak of TQ1 at 600 nm can be attributed to a combination of the intramolecular D-A charge transfer (ICT) and the intermolecular interactions between the polymeric chains since that upon heating at 100 °C the intermolecular interactions are preventing and a maximum absorption peak at 555 nm is observed which is assigned solely to ICT interactions.[15,16] Similar to TQ1, the absorption peak of T23TQ at 600 nm can be assigned to a combination of the ICT and the intermolecular interactions, respectively. On the other hand, the absorption peak of T32TQ at 616 nm in solution can safely be assigned to the ICT interactions, whereas the higher absorption band at 656 nm could safely attributed to vibronic transitions from the interchain interactions, similar to those observed for other conjugated polymers. Furthermore, the low-wavelength peak observed at 353 nm for T32TQ is situated at longer wavelengths than T23TQ (342 nm) showing that the selection of the T32T provides enhanced conjugation in the polymer backbone.

Figure 1.

Despite the fact that T23TQ and TQ1 reveal different molecular weights (Table 1) and different dihedral angles

(Figure S3 in SI), their absorption spectra are the same both in solution and in solid state, as mentioned previously. The identical absorption spectra and the same optical band gap (E_g^{opt}) of T23TQ and TQ1 are somehow surprising, since the simple DFT calculations (see Figure 4 next in the text) support a wider predicted band gap. Possible explanations are the different molecular backbone structure and the resonance structures of T23TQ and TQ1 or combination of them. T23TQ exhibits a more linear backbone in comparison to TQ1 – which has significant curvature (Figure 4). In addition, the resonance structures of the copolymers are presented in Figure 2. T23TQ demonstrates the same short conjugated segment as TQ1, due to the cross conjugation of T23T along the polymer backbone, therefore inhibits the full delocalization. On the contrary, T32T allows the full delocalization on T32TQ, hence T32TQ shows longer conjugated segment as compared to T23TQ and TQ1 and different absorption spectrum.

Figure 2.

Upon film formation the longer wavelength peak of T23TQ, T32TQ and TQ1 increases in intensity relative to solution and slightly red-shifts indicative of enhanced interchain interactions (Figure 1b). TQ1 and T23TQ exhibit higher absorption coefficient ($1x10^5$ cm^{-1}) at the maximum absorption peak as compared to T32TQ ($9x10^4$ cm^{-1}). The absorption maxima of the copolymers as thin films are red shifted as compared to solution. T23TQ and TQ1 exhibit absorption maxima at 627 nm, whereas T32TQ at 665 nm in solid state. The optical band gaps, as measured by the onset of UV-Vis absorption in the solid state are 1.75 eV for T23TQ and TQ1, and 1.68 eV for T32TQ. Finally, the trend on the low-wavelength peaks of the copolymers in the solid state is the same as in solution. T23TQ and TQ1 exhibit an absorption peak at 365 nm while T32TQ at 379 nm. The absorption spectra of TQ1:$PC_{70}BM$, T23TQ:$PC_{70}BM$ and T32TQ:$PC_{70}BM$ as thin films in various compositions (1:1, 1:2 and 1:3) were also recorded (Figure S4 in SI). Upon addition of $PC_{70}BM$ the absorption coefficient of all systems decreases, even in 1:1 ratio, as compared to pristine films (Figure 1). Furthermore, the intensity of the low energy absorption maximum peak decreases for the TQ1 and T32TQ, while T23TQ seems to be insensitive by the increment of the $PC_{70}BM$ content (Figure S4), whereas the absorption peak at around 500 nm (characteristic of the $PC_{70}BM$[18]) increases in all cases.

The emission spectra of the copolymers in solution are presented in Figure 1a. The emission spectra of T23TQ and TQ1 are identical in shape with the appearance of a maximum peak and a shoulder. However, the maximum emission peak at 671 nm and the shoulder at 722 nm of T23TQ are slightly red shifted as compared to TQ1 (667 nm the maximum emission peak and 715 nm the shoulder). On the other hand, T32TQ shows only a maximum emission peak at 695 nm without the appearance of a shoulder.

The energy levels of the copolymers were investigated by differential pulse voltammetry (DPV) in thin film form. The reduction potentials of TQ1, T23TQ and T32TQ are shown in Figure 3, while no obvious oxidation potentials were appeared for all the copolymers. The reduction peak potentials of TQ1, T23TQ and T32TQ versus Fc/Fc^+ are -1.64 V, -1.69 V and -1.53 V, respectively (Table 1) resulting in estimated LUMO energy levels (E_{LUMO}) of -3.49 eV (TQ1), -3.44 eV (T23TQ) and -3.60 eV (T32TQ) vs. vacuum as derived from the equation $E_{LUMO} = -5.1 + E_{peak}^{red}$ eV. Based on these results, someone can realize that the selection of the different isomeric structure of thienothiophene (T23T versus T32T) significantly influences the E_{LUMO} of these D-A copolymers, even though the electron accepting unit (quinoxaline) is the same. The incorporation of the cross conjugated T23T in the polymer backbone leads to upshifted LUMO level as compared to TQ1 and consequently to a lower electron affinity copolymer. Instead, the integration of the fully conjugated T32T in the polymer backbone drives the LUMO level to deeper values, as compared to TQ1, and therefore to a higher electron affinity copolymer. The reduction potentials of $PC_{60}BM$ have been also determined by cyclic voltammetry (Figure S5 in SI). The first reduction potential of PCBM is detected at -1.20 V versus Fc/Fc^+, resulting in an E_{LUMO} of -3.90 eV vs. vacuum. Thus, the E_{LUMO} offset (α) between the PCBM and the copolymers is calculated and is 0.41 eV for TQ1, 0.46 eV for T23TQ and 0.30 eV for T32TQ (Table 1).

Figure 3.

In order to gain more insights about the differences observed for the E_{LUMO} of the copolymers, quantum chemical (DFT) calculations[19] were performed to predict the molecular energy levels and model the distribution of the frontier molecular orbitals of the copolymers (Figure S6 in SI). The calculated LUMO energy levels of the tetramers following the same trend as the DPV. However distinct differences are observed in the shape of the molecular orbitals of the corresponding LUMO levels, which are related to the type of the thienothiophene isomeric form that is used. For example, the LUMO levels for both the model compounds of TQ1 and T32TQ assumes a more quinoidal form as shown by the presence of orbital lobes in the bonds between the thiophene and quinoxaline (TQ1) and T32T and quinoxaline (T32TQ) along with a significant localization of the LUMO on the quinoxaline unit. This orbital lobe pattern is similar to the HOMO of a series of thiophene oligomers that are quinoidal in the ground state.[20] On the contrary, the LUMO level of the model compound of T23TQ is mainly localized on the quinoxaline unit and the neighboring carbon atoms of T23T. In this case the quinoidal form is absent. Therefore, it seems that in these quinoxaline based D-A copolymers the use of thiophene or T32T (which are short and fully conjugated) enables the formation of the quinoidal structure, whereas the use of T23T (short and cross conjugated) prevents the formation of the quinoidal structure. As a conclusion, even if all the copolymers contain the same electron accepting unit (quinoxaline) and might be expected to show similar LUMO level values, the use of electron rich building blocks that contribute to the formation of the quinoidal structure on the LUMO levels results in D-A copolymers with enhanced electron affinities as compared to those electron rich monomers that prevent the formation of the quinoidal structure. Finally, it is possible to observe that in all three copolymers the HOMO level is fully delocalized along the polymer chain axis.

2.3. Structural (X-Ray) characterization

The ordering of drop cast films of the polymers was investigated by X-ray scattering (XRD) as shown in Figure 4. All polymers diffract rather weakly, but there are nevertheless distinct diffraction features in pure TQ1 and T23TQ films that are detected at 2θ = 4.21 Å, corresponding to a *d*-spacing of 21.0 nm. This diffraction peak in TQ1 has been attributed to an

ordered lamellar packing motif with a presumably edge-on orientation.[16] In contrast, there is no peak present for T32TQ which indicates a more amorphous structure. The combination of in and out of plane solubilising groups, as presented in Figure 4 for T32TQ, appears to frustrate the ordering of the polymer similar to the results presented elsewhere.[21-23]

Figure 4.

2.4. Charge Transporting Properties

2.4.1. Transistor Field-Effect measurements

Bottom-gate, bottom-contact (BG/BC) field-effect transistors were fabricated in order to investigate the charge transport characteristics of this series of copolymers. The transistor architecture used together with representative sets of the transfer characteristics of these devices are shown in Figure 5. All of the three pristine copolymers exhibited typical unipolar hole transporting (p-type) characteristics. The extracted hole mobility values measured in saturation regime are $4.0\times10^{-5}\pm3.1\times10^{-5}$ cm^2 $V^{-1}s^{-1}$ for TQ1, $3.0\times10^{-5}\pm7.8\times10^{-6}$ cm^2 $V^{-1}s^{-1}$ for T23TQ and $3.7\times10^{-7}\pm1.6\times10^{-7}$ cm^2 $V^{-1}s^{-1}$ for T32TQ. TQ1 and T23TQ yielded hole mobilities of the same order of magnitude, while T32TQ showed lowered mobility of about two orders of magnitude. The hole mobility results correlate well with the X-ray structural characterization, where T32TQ indicated a more disordered packing mode due to disrupted and weaker interaction between polymer chains.

Figure 5.

2.4.2. Space Charge Limited Current (SCLC) measurements

The charge transport properties of the pristine polymers and polymer:$PC_{70}BM$ blend films were also studied by utilizing the space charge limited current model. For each system, unipolar devices were fabricated and their dark J–V characteristics were recorded. For all systems studied, the carrier mobility values were determined based on the Mott-Gurney equation, by taking into account the Poole-Frenkel effect.[24] The dark J-V curves are presented in Figure S7 in SI. Table 2 summarizes the results of the charge transport characterization of all devices. The hole mobility of the pristine TQ1, T23TQ and T32TQ devices are calculated to be $4.5\times10^{-4}\pm1.7\times10^{-4}$, $5.3\times10^{-10}\pm2.0\times10^{-10}$ and $7.1\times10^{-9}\pm6.1\times10^{-9}$ cm^2 $V^{-1}s^{-1}$, respectively. The hole mobilities of T23TQ and T32TQ polymers are found comparatively very low as compared to TQ1 and are different to the results obtained on FETs. One possible explanation is that the two techniques measures the mobility of the charge carriers parallel (FETs) and perpendicular (SCLC) to the substrate. Since that TQ1 and T23TQ presumably exhibit an "edge on" orientation their FET mobilities are higher than that of T32TQ in agreement with the XRD analysis. On the other hand, it is unclear whether the orientation of the polymer chains is perpendicular to the substrate, hence advanced crystallographic techniques like 2D-GIWAXS, SAXS should be performed in order to obtain a full understanding of the polymer chain packing behaviour. Concerning the case of the polymer:$PC_{70}BM$ blends, with increasing $PC_{70}BM$ content both hole and electron mobility of the systems are found to increase, except in the case of TQ1, where the hole mobility decreases almost two order of magnitude.[25,26] This leads to more balanced hole and electron transport systems. Table 2 presents the extracted hole, electron mobility and the mobility ratios for the polymer:$PC_{70}BM$ blend systems in the different compositions.

Table 2.

2.5. Photovoltaic Performance

The photovoltaic properties of the TQ1:$PC_{70}BM$, T23TQ:$PC_{70}BM$ and T32TQ:$PC_{70}BM$ systems were tested in conventional OPV devices with the ITO/PEDOT:PSS/polymer:$PC_{70}BM$/Ca/Al geometry. For each polymer:$PC_{70}BM$ three different composition ratios (1:1, 1:2 and 1:3) were studied in order to identify the effect of increasing $PC_{70}BM$ content on the device performance. Figures 6a-c presents the photo J-V curves of these systems and Figures 6d-f presents the corresponding EQE spectra of these devices. Table 3 summarizes the findings of the electrical characterisation and presents the main output device characteristics of each system, that is the open circuit voltage (V_{oc}), the short-circuit current density (J_{sc}), the fill factor (FF) and the power conversion efficiency (PCE).

Figure 6.

The effect of increasing the $PC_{70}BM$ content is different in the three polymer:$PC_{70}BM$ OPV systems. Notably, the increase of $PC_{70}BM$ results in an increase of the PCE in the case of the TQ1:$PC_{70}BM$ system, where an average PCE of 5.7% and a maximum PCE of 6.6% are obtained for the composition ratio of 1:3. This result is in accordance with the PCE obtained by *Wang et el.*[15] and *Kim et al.*[16]. The effect is different in the case of the T23TQ:$PC_{70}BM$ and the T32TQ:$PC_{70}BM$. In the former, doubling the relative $PC_{70}BM$ content does not affect the device performance but for the 1:3 ratio the device efficiency decreases. A PCE of 5.0% is obtained for the T23TQ:$PC_{70}BM$ in 1:2 ratio. In the T32TQ:$PC_{70}BM$, doubling the relative $PC_{70}BM$ content is found to slightly increase the device PCE but for the 1:3 ratio the device efficiency is again reduced exhibiting device characteristics close to the device with the 1:1 ratio. A maximum PCE of 5.0% is obtained for the T32TQ:$PC_{70}BM$ in 1:2 ratio.

Table 3.

The results presented in Table 3 indicate that the observed trends in device performance of these systems are a consequence of the variation of the FF and the J_{sc} parameters of the cells as the polymer:$PC_{70}BM$ composition alters. It is very likely that the change of the $PC_{70}BM$ content influences the morphology of the OPV blend so that the charge carrier properties varies, hence the collection of the photogenerated charges is influenced accordingly. In addition, the change in the J_{sc} values for different $PC_{70}BM$ content implies that the amount of $PC_{70}BM$ in the blend results in changes in the charge carrier generation efficiency. The composition dependent device study of the T23TQ:$PC_{70}BM$ and T32TQ:$PC_{70}BM$ systems found that the optimum blending ratio for both systems is 1:2. Table 2 shows that in respect to the rest of the compositions tested, the hole/electron mobility ratio is balanced for the 1:2 mixing ratio. However by comparing the J_{sc} of the two systems at each composition, it is found that the T23TQ:$PC_{70}BM$ system outperforms the T32TQ:$PC_{70}BM$ system, regardless of how the charge transport is balanced in the blends.

Apart from the necessity for balanced charge transport, photocurrent generation depends also on the extent of phase

separation between the polymer matrix and the $PC_{70}BM$ component. Extended phase separation of the blend components leads to inefficient exciton dissociation whereas fine mixing of the blend components is detrimental to the efficiency of full charge separation due to the prevalence of charge recombination. We have studied the surface topography of the TQ1:$PC_{70}BM$, T23TQ:$PC_{70}BM$ and T32TQ:$PC_{70}BM$ blend films in their optimized composition ratio by Atomic Force Microscopy (AFM) (Figure 7) and it is found that the T23TQ:$PC_{70}BM$ exhibits an optimum phase separation with the formation of domains of 5-10 nm size, similar to TQ1:$PC_{70}BM$. In contrast the surface topography of the T32TQ:$PC_{70}BM$ suggests larger degree of phase separation for the T32TQ and $PC_{70}BM$ components that results in the formation of larger size domains of 10-20 nm.

Figure 7.

In each of the three systems when the mixing ratio is changed the device photocurrent is optimized because the mobility ratio is optimized. However this is not the case when different systems are compared. Therefore the comparison of the three different systems finds that balanced mobility ratio is not the key-parameter that determines the efficiency of device photocurrent. AFM images suggest that morphology variations in the three systems lead to different domain sizes that are likely to effect the process of charge photogeneration.

In agreement with the photo J-V curves, the EQE spectra in Figures 9d-f show that the TQ1:$PC_{70}BM$ 1:3 exhibits the highest photocurrent generation efficiency of all studied systems. According to the registered EQE spectra of all devices, both the polymer and $PC_{70}BM$ components contribute to the overall photocurrent generation efficiency. The EQE values are in full agreement with the device photocurrent measured under simulated solar illumination. We have calculated the expected J_{sc} values based on the registered external quantum efficiency (EQE) spectra of the studied systems. Table S4 (SI) compares the experimentally determined J_{sc} values as recorded under simulated solar illumination with the corresponding values as calculated by the EQE spectra. An excellent agreement is found between the two J_{sc} values indicating that the recorded EQE spectra reflect realistic results. The device V_{oc} remains nearly unaffected by the change in the polymer:$PC_{70}BM$ ratio used in each blend. In all cases the variation of the V_{oc} values is below 8%.

3. Conclusions

In summary, isomeric series of thienothiophene containing D-A copolymers utilizing bis(3-octyloxy)phenyl)quinoxaline have been successfully synthesized by Stille cross coupling polymerization procedure. By UV-vis spectroscopy, it has been shown that the optical gap of the cross-conjugated T23T based copolymer is higher than that of the fully-conjugated T32T and the absorption profiles of T23TQ are the same as TQ1 both in solution and the solid state. T32TQ exhibits higher electron affinity than T23TQ due to the presence of the quinoid form along the LUMO level. T23T enables the corresponding T23TQ to obtain higher degree of structural order than T32T in T32TQ with the appearance of a lamellar packing motif with a presumably edge-on orientation. The FET hole mobilities providing two order of magnitude enhanced hole mobilities for the T23TQ as compared to T32TQ. The photovoltaic performance of T23TQ and T32TQ shows that both copolymers exhibit similar PCE of around 5.0% with low loading of $PC_{70}BM$, despite the fact of their differences on optical, electrochemical, structural and charge transporting properties. However, even if the maximum PCE of the two isomeric polymers is the same, distinct differences in device photocurrents occur that are primary related to the different domain sizes of the blend films rather than the balanced mobility ratio.

4. Experimental Section

All reactions were treated as air and light sensitive and performed under argon and in the dark. All glassware used were washed using teepol surfactant, rinsing with excess water, acetone and methylene dichloride and dried in an oven at 120 °C. All solvents and reagents were sourced commercially from Aldrich. The synthesis of 5,8-dibromo-2,3-bis(3-(octyloxy) phenyl)quinoxaline, 2,5-bis(trimethylstannyl)thieno[3,2-*b*] thiophene, 2,5-bis(trimethylstannyl)thieno[2,3-*b*]thiophene and were performed according to the previously reported literature.[27-29]

Synthesis of TQ1: 2,5-bis(trimethylstannyl)thiophene (0.5 mmol, 204.88 mg) and 5,8-dibromo-2,3-bis(3-(octyloxy)phenyl)quinoxaline (0.5 mmol, 348.29 mg) were dissolved in dry toluene (25 mL). Then, tris(dibenzylideneacetone)dipalladium(0) (Pd_2dba_3) (0.005 mmol, 4.58 mg) and tri(*o*-tolyl)phosphine (P(*o*-tol)$_3$) (0.01 mmol, 3.04 mg) were added and the reaction mixture was stirred at 110°C under argon atmosphere for 17h. Then, the toluene solution was evaporated, the mixture was solubilised in $CHCl_3$. The polymer was purified by precipitation in methanol, filtered and washed on Soxhlet apparatus with methanol, ethyl acetate and chloroform. The chloroform fraction was evaporated under reduced pressure and the polymer was precipitated in acetone, filtered and finally dried under high vacuum, providing a dark blue solid with a metallic shine with 88 % of yield. The ^{1}H-NMR and GPC profile are presented on the supporting information file (Figure S9 and Figure S10 in SI).

Synthesis of T23TQ: 2,5-bis(trimethylstannyl)thieno[2,3-*b*]thiophene (0.5 mmol, 232.92 mg) and 5,8-dibromo-2,3-bis(3-(octyloxy)phenyl)quinoxaline (0.5 mmol, 348.29 mg) were dissolved in dry toluene (25 mL). Then, Pd_2dba_3 (0.005 mmol, 4.58 mg) and P(*o*-tol)$_3$) (0.01 mmol, 3.04 mg) were added and the reaction mixture was stirred at 110°C under argon atmosphere for 17h. Then, the toluene solution was evaporated, the mixture was solubilised in $CHCl_3$. The polymer was purified by precipitation in acetone, filtered and washed on Soxhlet apparatus with methanol, hexane and chloroform. The chloroform fraction was evaporated under reduced pressure and the polymer was precipitated in acetone, filtered and finally dried under high vacuum, providing a dark blue solid with 70 % of yield. The ^{1}H-NMR and GPC profile are presented on the supporting information file (Figure S9 and Figure S10 in SI).

Synthesis of T32TQ: 2,5-bis(trimethylstannyl)thieno[3,2-*b*]thiophene (0.5 mmol, 232.92 mg) and 5,8-dibromo-2,3-bis(3-(octyloxy)phenyl)quinoxaline (0.5 mmol, 348.29 mg) were dissolved in dry toluene (25 mL). Then, Pd_2dba_3 (0.005 mmol, 4.58 mg) and P(*o*-tol)$_3$) (0.005 mmol, 3.04 mg) were added and the reaction mixture was stirred at 110°C under argon atmosphere for 17h. Then, the toluene solution was evaporated, the mixture was solubilised in $CHCl_3$. The polymer was purified by precipitation in acetone, filtered and washed on Soxhlet apparatus with methanol, hexane and chloroform. The chloroform fraction was evaporated under reduced pressure and

the polymer was precipitated in acetone, filtered and finally dried under high vacuum, providing a dark blue solid with 81 % of yield. The ^{1}H-NMR and GPC profile are presented on the supporting information file (Figure S9 and Figure S10 in SI).

Nuclear Magnetic Resonance (NMR): ^{1}H and ^{13}C NMR spectra were recorded on a Bruker AV-400 (400 MHz for ^{1}H and 100 MHz for ^{13}C), using the residual solvent resonance of $CDCl_3$ as an internal reference.

Gel Permeation Chromatography (GPC): Molecular weights (M_n and M_w) were determined by GPC (Ultrastyragel columns with 500 and 10^4 Å pore size; $CHCl_3$ (analytical grade) was filtered through a 0.2 μm Millipore filter; flow 1 mL min^{-1}; room temperature) using narrow polystyrene standards for calibration.

Thermogravimetric Analysis: The thermogravimetric analysis was performed using a TGA Q500 V20.2 Build 27 instrument by TA in an inert atmosphere of nitrogen. In a typical experiment 2 mg of the material was placed in the sample pan and the temperature was equilibrated at 40 ^{o}C. Subsequently, the temperature was increased to 800 ^{o}C with a rate of 10 ^{o}C/min and the weight changes were recorded as a function of temperature.

Differential Pulse Voltammetry (DPV): Electrochemistry studies were performed by using a standard three-electrode cell. Platinum wire was used as a pseudo-reference electrode, platinum disk 1.6 mm diameter was used as a working electrode and platinum, 52 mesh, was used a counter electrode. $TBAPF_6$ (98%) was used as the electrolyte and was recrystallized three times from acetone and dried in a vacuum at 100 ^{o}C. Before each experiment the cell was purged with high purity N_2 for 5 min. Before the start of the measurement the inert gas was turned to "blanket mode". Measurements were recorded by using an EG&G Princeton Applied Research potensiostat/galvanostat Model 2273 connected to a personal computer running PowerSuite software. The working electrode was cleaned before each experiment through polishing using a cloth and 6, 3, and 1 mm diamond pastes. DPV experiments where performed by using pulse PH/PW: 0.025V/ 20ms, step time 40ms and a scan rate 50mV/s. All measurements were taken in room temperature and were calibrated by using ferrocene as internal standard.

Theoretical Calculations: All calculations of the model compounds studied in this work have been performed using the Gaussian 03 software package.[19] The octyloxy substituents anchored onto the peripheral phenyl rings of quinoxaline have been replaced with methoxy groups in the model compounds for our calculations. While the presence of these long alkyl chains enhances the solubility of these polymers and affect the charge carrier mobility and photovoltaic behavior of the polymer,[30] from a computational point of view their replacement with shorter chains does not affect their optoelectronic properties (HOMO, LUMO and band gap) and thus the optimized structures of the molecules.[31] The ground-state geometry of each model compound has been determined by a full geometry optimization of its structural parameters using the DFT, upon energy minimization of all possible isomers. In this work, the DFT calculations were performed using the Becke's three-parameter hybrid functional, B3, with non-local correlation of Lee-Yang-Parr, LYP, abbreviated as B3LYP in conjunction with the 6-31G(d,p) split valence polarized basis set. All calculations were performed in vacuum. No symmetry constraints were imposed during the optimization process. The geometry optimizations have been performed with a tight threshold that corresponds to root mean square (rms) residual forces smaller than 10^{-5} au for the optimal geometry. The energy level of the HOMO and the LUMO of the repetitive units of each polymer were carried out by using the same set of calculations. DFT/B3LYP/6-31G(d,p) has been found[10c] to be an accurate formalism for calculating the structural and electronic properties of many molecular systems. In our studies the theoretical calculations performed on tetramer model compounds. The visualization of the molecular orbitals has been performed using GaussView 5.0.

Solution and Thin film prepration: The solutions of polymer (either TQ1 or T23TQ or T32TQ): phenyl-C_{71}-butyric acid methyl ester ($PC_{70}BM$) blend were prepared in 1,2-dichlorobenzene (DCB) solvent in a N_2-filled glovebox. Three different compositions were tested; 1:1 (22mg/mL), 1:2 (24mg/mL) and 1:3 (28mg/mL). The solutions were stirred for 48 hours at 100 ^{o}C to get a clear solution and were deposited by spin-coating on quartz subsrates for spectroscopic studies. Surface profilometry (Bruker, D150) was used for determining the film thickness and for optimizing the thickness of the blend films.

Time integrated UV absorption and photoluminescence spectroscopy: UV-vis absorption and photoluminescence spectra of the blend films were recorded with a Perkin Elmer, Lambda 1050 spectrometer and a Horiba Jobin Yvon NanoLog spectrofluorimeter, respectively.

X-Ray characterization: X-ray diffraction (XRD) measurements were performed on the PANALYTICAL X′ PERT-PRO MRD diffractometer equipped with nickel-filtered Cu Kα1 beam and X′ CELERATOR detector, using current I = 40 mA and accelerating voltage V = 40 kV. Samples were prepared by drop casting.

Organic field effect transistor (OFET) fabrication: Fraunhofer substrates, bottom gate/bottom contact architecture with ~230 nm n-doped SiO_2 as gate dielectric, were cleaned with acetone, water and isopropanol for 15 min, respectively, under ultrasonication. The substrates were blow dried with nitrogen before being treated with UV ozone for 15 min. The substrates were then modified with Hexamethyldisilazane (HMDS). The polymers were dissolved in 1,2-dichlorobezene by stirring for 48 h at 100 ^{o}C to reach the concentration of 16 mg/mL for TQ1, 20 mg/mL for T23Q and 20 mg/mL for T32Q. The semiconductor layer was then spin coated from the polymer solution at 900 rpm for 120 s at room temperature. The solvent residue was removed under vacuum before the devices were tested with an Agilent B2902A source/measure unit. The channel width and length of the transistors are 10 mm and 10 µm, respectively. Mobility was extracted from the slope of $I_D^{1/2}$ vs. V_G.

Space Charge Limited Current (SCLC) measurements: Single carrier devices with photoactive layers were prepared in identical fashion as in the case of the OPV devices. Electron-only devices were prepared with electrodes of glass/ITO/ZnO and Ca/Al, whereas hole only devices were prepared with electrodes of glass/ITO/PEDOT:PSS and Au. Dark J-V characteristics of the fabricated single carrier devices were recorded with a 2440 Keithley source-measure unit. The determination of the charge carrier mobility for each device was based on the space charge limited current mode like previously described.[24]

Solar cell fabrication and characterization: Solar cell devices were fabricated by depositing a 90 nm-thick polymer:$PC_{70}BM$ blend films onto glass/Indium Tin Oxide (ITO)/poly(3,4-ethylenedioxythiophene):polystyrensulfonate (PEDOT:PSS) substrates by spin-coating in a N_2-filled glovebox. Prior to

PEDOT:PSS deposition, the ITO substrates (Xin Yan Technology Ltd, sheet resistance - 15 Ω/square) were ultrasonically cleaned using acetone and isopropanol. They were then treated with Hellmanex III surfactant to remove contaminants and residues from the ITO surface and were cleaned again with succesive 15 min-long cycles of ultrasonication in deionized water, acetone and isopropanol. The cleaned ITO susbtrates were oxygen plasma etched at 100W for 10 min and a 40 nm thick PEDOT:PSS layer was deposited by spin coating in air. The glass/ITO/PEDOT:PSS film is dried in air at 150 °C for 30 minutes. Following the deposition of the polymer:$PC_{70}BM$ photoactive layers the metal electrode of Ca/Al was deposited by thermal evaporation in vacuum (1×10^{-6} m bar) onto the top of photoactive film by using a prepattrened shadow mask. The obtained OPV devices were encapsulated with degassed epoxy and 1 mm thick glass slides inside the N_2-glove box. The electrical characterization of the solar cell devices was performed by means current density-voltage (J-V) characteristics recorded under simulated solar light (AM1.5G, 0.98 Sun) and by registering the external quantum efficiency (EQE) spectra under monochromated light. For each system at least four to six devices were characterized for confirming the reproducibility of the obtained results.

Atomic Force Microscopy (AFM): AFM images were obtained with a Picoscan PicoSPM LE scanning probe in tapping mode under ambient conditions. Thin films of polymer blends were fabricated following identically the same procedure as the OPV device fabrication, except that the evaporation of electrodes was not performed.

Acknowledgements

CLC and GP would like to thank the Ministry of Education and Religious Affairs in Greece for the financial support of this work provided under the co-operational program "AdvePol: E850" project. This project has received funding from the European Community's Seventh Framework Programme (FP7/2007-2013) under the Grant Agreement n° 331389. CLC acknowledges the financial support of a Marie Curie Intra European Fellowship (FP7-PEOPLE-2012-IEF) project ECOCHEM. The theoretical calculations in this study were performed at the Research Center for Scientific Simulations (RCSS) at the University of Ioannina. The authors would like to thank Associate Professor Elefterios Lidorikis of Department of Materials Science and Engineering, University of Ioannina for his assistance in the theoretical calculations.

Notes and references

[1] Center for Nano Science and Technology@Polimi, Istituto Italiano di Tecnologia, via Pascoli 70/3, 20133 Milano, Italy.
[2] Advent Technologies SA, Patras Science Park, Stadiou Street, Platani-Rio, 26504, Patra, Greece, E-mail: cchochos@advent-energy.com
[3] Theoretical and Physical Chemistry Institute, National Hellenic Research Foundation, 48 Vassileos Constantinou Avenue, Athens 11635, Greece.
[4] Department of Chemistry and Centre for Plastic Electronics, Imperial College London, Exhibition Road, South Kensington, London SW7 2AY, UK.
[5] Department of Materials Science Engineering, University of Ioannina, Ioannina 45110, Greece, E-mail: cchochos@cc.uoi.gr
[6] Department of Physics and Centre for Plastic Electronics, Imperial College London, Exhibition Road, South Kensington, London SW7 2AY, UK.
[7] Department of Mechanical Engineering and Materials Science and Engineering, Cyprus University of Technology, Dorothea Bldg, 5th floor, 45 Kitiou Kyprianou Str., Limassol 3041, Cyprus, E-mail: p.keivanidis@cut.ac.cy

† Electronic Supplementary Information (ESI) available. See DOI: 10.1039/b000000x/

1 A. J. Heeger, *Adv. Mater.*, 2014, **26**, 10.
2 X. Guo, M. Baumgarten and K. Müllen, *Prog. Polym. Sci.*, 2013, **38**, 1832.
3 C. L. Chochos and S. A. Choulis, *Prog. Polym. Sci.*, 2011, **36**, 1326.
4 P. M. Beaujuge and J. M. J. Fréchet, *J. Am. Chem. Soc.*, 2011, **133**, 20009.
5 J. Roncali, *Macromol. Rapid Commun.*, 2007, **28**, 1761.
6 P.-L. T. Boudreault, A. Najari and M. Leclerc, *Chem. Mater.*, 2011, **23**, 456; A. Facchetti, *Chem. Mater.*, 2011, **23**, 733.
7 J. E. Anthony, A. Facchetti, M. Heeney, S. R. Marder and X. Zhan, *Adv. Mater.*, 2010, **22**, 3876.
8 T. Lei, J.-Y. Wang and J. Pei, *Chem. Mater.*, 2014, **26**, 594; L. Biniek, S. Fall, C. L. Chochos, D. V. Anokhin, D. A. Ivanov, N. Leclerc, P. Lévêque and T. Heiser, *Macromolecules*, 2010, **43**, 9779.
9 Y. Shin, J. Liu, J. J. Quigley IV, H. Luo and X. Lin, *ACS Nano,* 2014, **8**, 6089.
10 B. Kippelen and J.-L. Brédas, *Energy Environ. Sci.*, 2009, **2**, 251; C. L. Chochos, A. Avgeropoulos and E. Lidorikis, *J. Chem. Phys.*, 2013, **138**, 064901; L. Pandey, C. Risko, J. E. Norton and J.-L. Brédas, *Macromolecules,* 2012, **45**, 6405.
11 H. Zhou, L. Yang and W. You, *Macromolecules,* 2012, **45**, 607.
12 R. Rieger, D. Beckmann, A. Mavrinskiy, M. Kastler and K. Müllen, *Chem. Mater.*, 2010, **22**, 5314.
13 I. McCulloch, M. Heeney, M. L. Chabinyc, D. DeLongchamp, R. Joseph Kline, M. Cölle, W. Duffy, D. Fischer, D. Gundlach, B. Hamadani, R. Hamilton, L. Richter, A. Salleo, M. Shkunov, D. Sparrowe, S. Tierney and W. Zhang, *Adv. Mater.*, 2009, **21**, 1091.
14 I. Osaka, T. Abe, S. Shinamura and K. Takimiya, *J. Am. Chem. Soc.*, 2011, **133**, 6852.
15 E. Wang, L. Hou, Z. Wang, S. Hellström, F. Zhang, O. Inganäs and M. R. Andersson, *Adv. Mater.*, 2010, **22**, 5240.
16 Y. Kim, H. R. Yeom, J. Y. Kim and C. Yang, *Energy Environ. Sci.*, 2013, **6**, 1909.
17 E. Wang, J. Bergqvist, K. Vandewal, Z. Ma, L. Hou, A. Lundin, S. Himmelberger, A. Salleo, C. Müller, O. Inganäs, F. Zhang and M. R. Andersson, *Adv. Energy Mater.*, 2013, **3**, 806.
18 M. M. Wienk, J. M. Kroon, W. J. H. Verhees, J. Knol, J. C. Hummelen, P. A. van Hal and R. A. J. Janssen, *Angew. Chem. Int. Ed.*, 2003, **42**, 3371.
19 M. J. Frisch, G. W. Trucks, H. B. Schlegel, G. E. Scuseria, M. A. Robb, J. R. Cheeseman, J. A. Montgomery, Jr., T. Vreven, K. N. Kudin, J. C. Burant, J. M. Millam, S. S. Iyengar, J. Tomasi, V. Barone, B. Mennucci, M. Cossi, G. Scalmani, N. Rega, G. A. Petersson, H. Nakatsuji, M. Hada, M. Ehara, K. Toyota, R. Fukuda, J. Hasegawa, M. Ishida, T. Nakajima, Y. Honda, O. Kitao, H. Nakai, M. Klene, X. Li, J. E. Knox, H. P. Hratchian, J. B. Cross, V. Bakken, C. Adamo, J. Jaramillo, R. Gomperts, R. E. Stratmann, O. Yazyev, A. J. Austin, R. Cammi, C. Pomelli, J. W. Ochterski, P. Y. Ayala, K. Morokuma, G. A. Voth, P. Salvador, J. J. Dannenberg, V. G. Zakrzewski, S. Dapprich, A. D. Daniels, M. C. Strain, O. Farkas, D. K. Malick, A. D. Rabuck, K. Raghavachari, J. B. Foresman, J. V. Ortiz, Q. Cui, A. G. Baboul, S. Clifford, J. Cioslowski, B. B. Stefanov, G. Liu, A. Liashenko, P. Piskorz, I. Komaromi, R. L.

Martin, D. J. Fox, T. Keith, M. A. Al-Laham, C. Y. Peng, A. Nanayakkara, M. Challacombe, P. M. W. Gill, B. Johnson, W. Chen, M. W. Wong, C. Gonzalez and J. A. Pople, GAUSSIAN 03, Revision E.01, Gaussian, Inc., Wallingford, CT, 2004.

20 J. Casado, M. Z. Zgierski, P. C. Ewbank, M. W. Burand, D. E. Janzen, K. R. Mann, T. M. Pappenfus, A. Berlin, E. Perez-Inestrosa, R. P. Ortiz and J. T. L. Navarrete, *J. Am. Chem. Soc.*, 2006, **128**, 10134.

21 C. P. Yau, Z. Fei, R. S. Ashraf, M. Shahid, S. E. Watkins, P. Pattanasattayavong, T. D. Anthopoulos, V. G. Gregoriou, C. L. Chochos and M. Heeney, *Adv. Funct. Mater.*, 2014, **24**, 678.

22 A. Salleo, R. J. Kline, D. M. DeLongchamp and M. L. Chabinyc, *Adv. Mater.*, 2010, **22**, 3812.

23 J. Rivnay, S. C. B. Mannsfeld, C. E. Miller, A. Salleo and M. F. Toney, *Chem. Rev.*, 2012, **112**, 5488.

24 F. Machui, S. Rathgeber, N. Li, T. Ameri and C. J. Brabec, *J. Mater. Chem.*, 2012, **22**, 15570.

25 L. M. Andersson, F. L. Zhang and O. Inganas, *Appl. Phys. Lett.*, 2007, **91**, 071108.

26 S. M. Tuladhar, D. Poplavskyy, S. A. Choulis, J. R. Durrant, D. D. C. Bradley and J. Nelson, *Adv. Func. Mater.*, 2005, **15**, 1171.

27 A. Gadisa, W. Mammo, L. M. Andersson, S. Admassie, F. Zhang, M. R. Andersson and O. Inganäs, *Adv. Funct. Mater.*, 2007, **17**, 3836.

28 I. McCulloch, M. Heeney, C. Bailey, K. Genevicius, I. MacDonald, M. Shkunov, D. Sparrowe, S. Tierney, R. Wagner, W. Zhang, M. L. Chabinyc, R. J. Kline, M. D. McGehee and M. F. Toney, *Nature Mater.*, 2006, **5**, 328.

29 M. Heeney, C. Bailey, K. Genevicius, M. Shkunov, D. Sparrowe, S. Tierney and I. McCulloch, *J. Am. Chem. Soc.*, 2005, **127**, 1078.

30 H. Bronstein, D. S. Leem, R. Hamilton, P. Woebkenberg, S. King, W. Zhang, R. S. Ashraf, M. Heeney, T. D. Anthopoulos, J. de Mello and I. McCulloch, *Macromolecules*, 2011, **44**, 6649; L. Biniek, C. L. Chochos, N. Leclerc, O. Boyron, S. Fall, P. Lévêque and T. Heiser, *J. Polym. Sci. Part A: Polym. Chem.*, 2012, **50**, 1861; L. Biniek, S. Fall, C. L. Chochos, N. Leclerc, P. Lévêque and T. Heiser, *Org. Electron.*, 2012, **13**, 114.

31 J. Ku, Y. Lansac and Y. H. Jang, *J. Phys. Chem. C*, 2011, **115**, 21508; C. Risko, M. D. McGehee and J.-L. Brédas, *Chem. Sci.*, 2011, **2**, 1200.

Scheme 1. Synthetic routes toward the preparation of the D-A copolymers TQ1, T32TQ and T23TQ

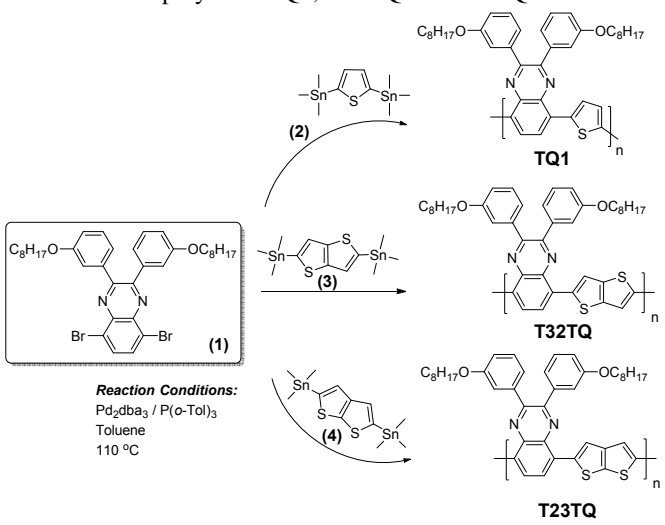

Table 1. Molecular weight characteristics, optical and electrochemical properties of TQ1, T23TQ and T32TQ.

Samples	M_n (g/mol)	PDI	λ_{max}^{sol} (nm)	λ_{max}^{film} (nm)	E_g^{opt} (eV)	Pl_{max}^{sol} (nm)	E_{red} (V)	E_{LUMO} (eV)	α (eV)
TQ1	33000	2.6	342, 600	365, 627	1.75	667, 715	-1.64	-3.49	0.41
T23TQ	20000	2.0	342, 600	365, 627	1.75	671, 722	-1.69	-3.44	0.46
T32TQ	20000	2.0	353, 616, 656	379, 620, 665	1.68	695	-1.53	-3.60	0.30

LUMO offset between the polymers and the fullerene derivative PCBM ($\alpha = E_{LUMO}^{PCBM} - E_{LUMO}^{pol}$)

Figure 1. (a) Absorption and emission spectra of TQ1, T23TQ and T32TQ in ortho-dichlorobenzene solution, and (b) absorption spectra of TQ1, T23TQ and T32TQ in the solid state.

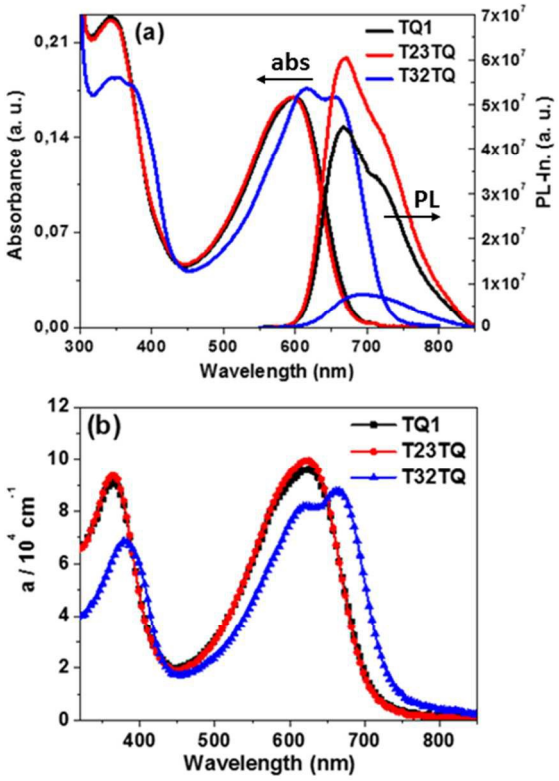

Figure 2. Resonance structures of TQ1, T23TQ and T32TQ. With blue color it is shown the short conjugated segments of TQ1 and T23TQ, and with red color the longer conjugated segment of T32TQ.

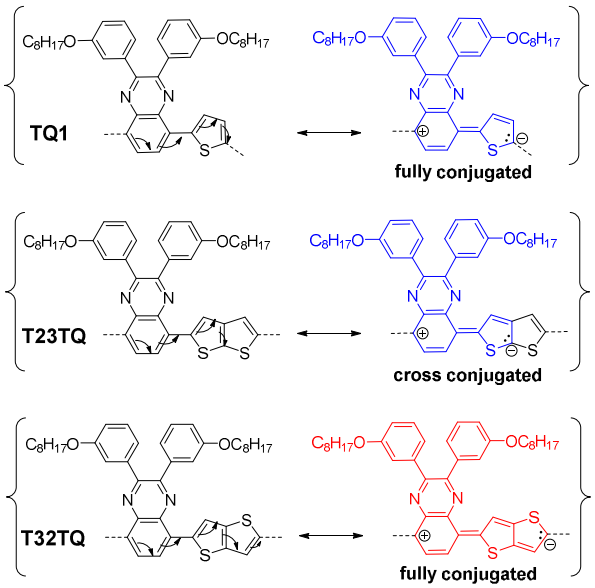

Figure 3. Reduction potentials of TQ1, T23TQ and T32TQ obtained by differential pulse voltammetry (DPV) as thin films.

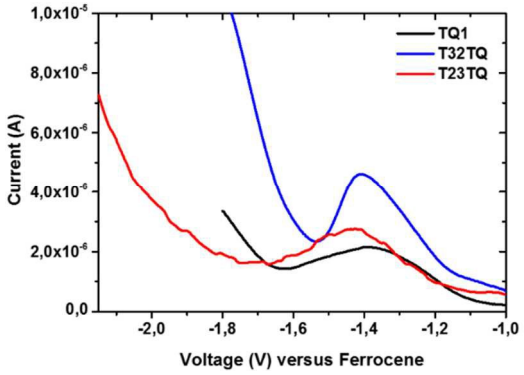

Figure 4. X-Ray diffraction patterns of TQ1, T23TQ and T32TQ films drop cast from chlorobenzene

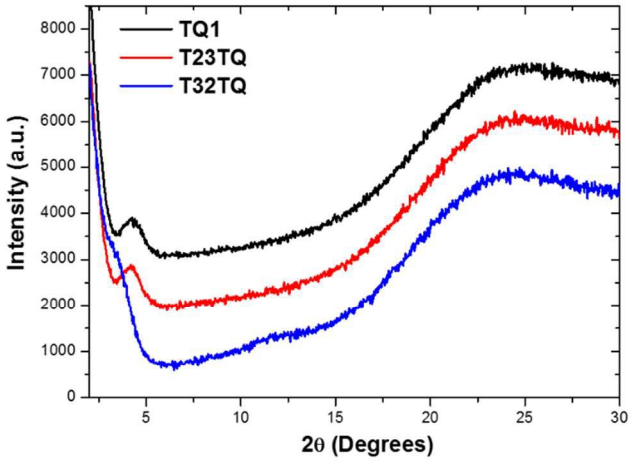

Figure 5. Transfer characteristics of TQ1, T23TQ and T32TQ based transistors measured in nitrogen at room temperature.

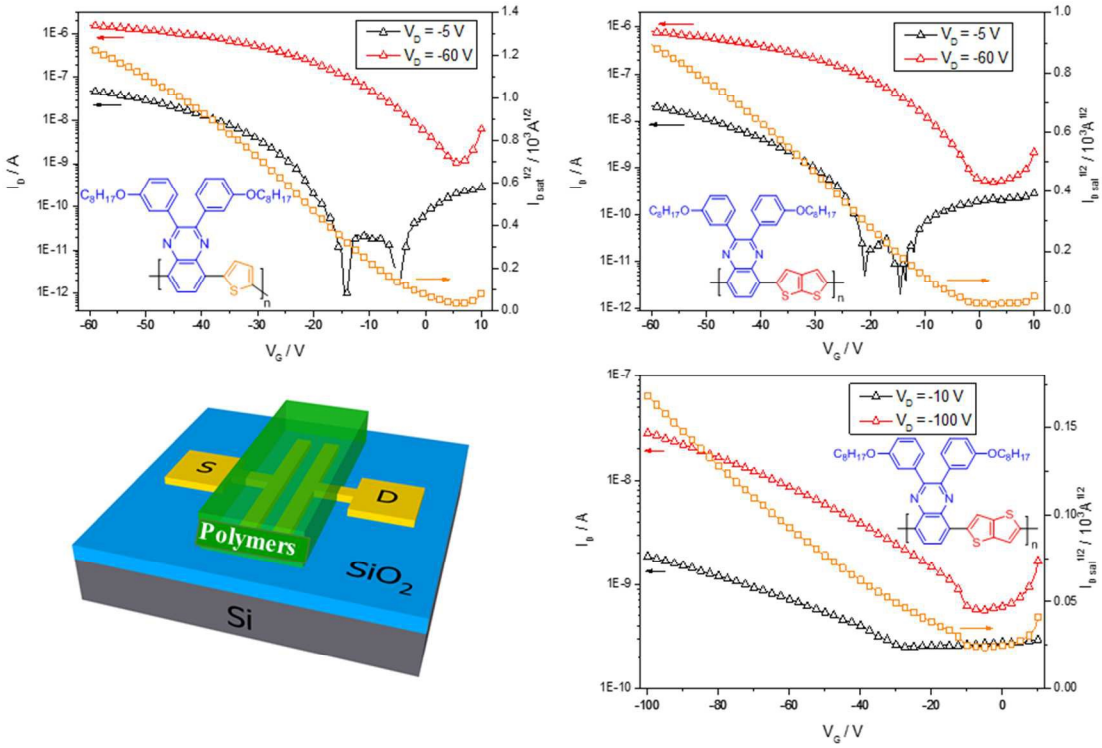

Table 2. Space charge carrier limited hole and electron mobility values as determined for the polymer-alone and the polymer:$PC_{70}BM$ blend films.

Blend System	μ_h ($cm^2 V^{-1} s^{-1}$)	μ_e ($cm^2 V^{-1} s^{-1}$)	μ_h / μ_e	J_{sc} (mA/cm^2)
TQ1	$4.5\times10^{-4} \pm 1.7\times10^{-4}$	-	-	-
TQ1:$PC_{70}BM$ (1:1)	$1.6\times10^{-6} \pm 4.9\times10^{-7}$	$2.4\times10^{-8} \pm 1.4\times10^{-8}$	66.6	7.5 ± 0.32
TQ1:$PC_{70}BM$ (1:2)	$3.5\times10^{-6} \pm 1.7\times10^{-6}$	$7.5\times10^{-7} \pm 3.2\times10^{-7}$	4.7	8.6 ± 0.19
TQ1:$PC_{70}BM$ (1:3)	$7.8\times10^{-6} \pm 1.8\times10^{-6}$	$9.0\times10^{-7} \pm 4.1\times10^{-7}$	8.7	9.4 ± 1.45
T23TQ	$5.3\times10^{-10} \pm 2.0\times10^{-10}$	-	-	-
T23TQ:$PC_{70}BM$ (1:1)	$9.6\times10^{-6} \pm 4.6\times10^{-6}$	$5.3\times10^{-7} \pm 1.8\times10^{-8}$	18.1	8.5 ± 0.02
T23TQ:$PC_{70}BM$ (1:2)	$2.1\times10^{-5} \pm 1.7\times10^{-5}$	$3.5\times10^{-6} \pm 2.0\times10^{-6}$	6.0	9.6 ± 0.02
T23TQ:$PC_{70}BM$ (1:3)	$2.0\times10^{-4} \pm 2.2\times10^{-5}$	$1.0\times10^{-6} \pm 4.6\times10^{-6}$	200.0	8.5 ± 0.17
T32TQ	$7.1\times10^{-9} \pm 6.1\times10^{-9}$	-	-	-
T32TQ:$PC_{70}BM$ (1:1)	$7.9\times10^{-7} \pm 2.7\times10^{-7}$	$1.1\times10^{-6} \pm 3.5\times10^{-7}$	0.7	7.8 ± 0.06
T32TQ:$PC_{70}BM$ (1:2)	$1.1\times10^{-6} \pm 5.9\times10^{-8}$	$1.1\times10^{-6} \pm 4.9\times10^{-7}$	1.0	8.1 ± 0.65
T32TQ:$PC_{70}BM$ (1:3)	$2.2\times10^{-5} \pm 6.8\times10^{-6}$	$3.6\times10^{-6} \pm 1.5\times10^{-6}$	6.1	6.9 ± 0.58

Figure 6. J-V characteristics of the OPV devices for a) TQ1:$PC_{70}BM$, b) T23TQ:$PC_{70}BM$ and c) T32TQ:$PC_{70}BM$ in three different composition ratio [1:1 (black square), 1:2 (red circle) and 1:3 (blue triangle). EQE spectra of the OPV devices for d) TQ1:$PC_{70}BM$, e) T23TQ:$PC_{70}BM$ and f) T32TQ:$PC_{70}BM$ in three different composition ratio [1:1 (black square), 1:2 (red circle) and 1:3 (blue triangle)].

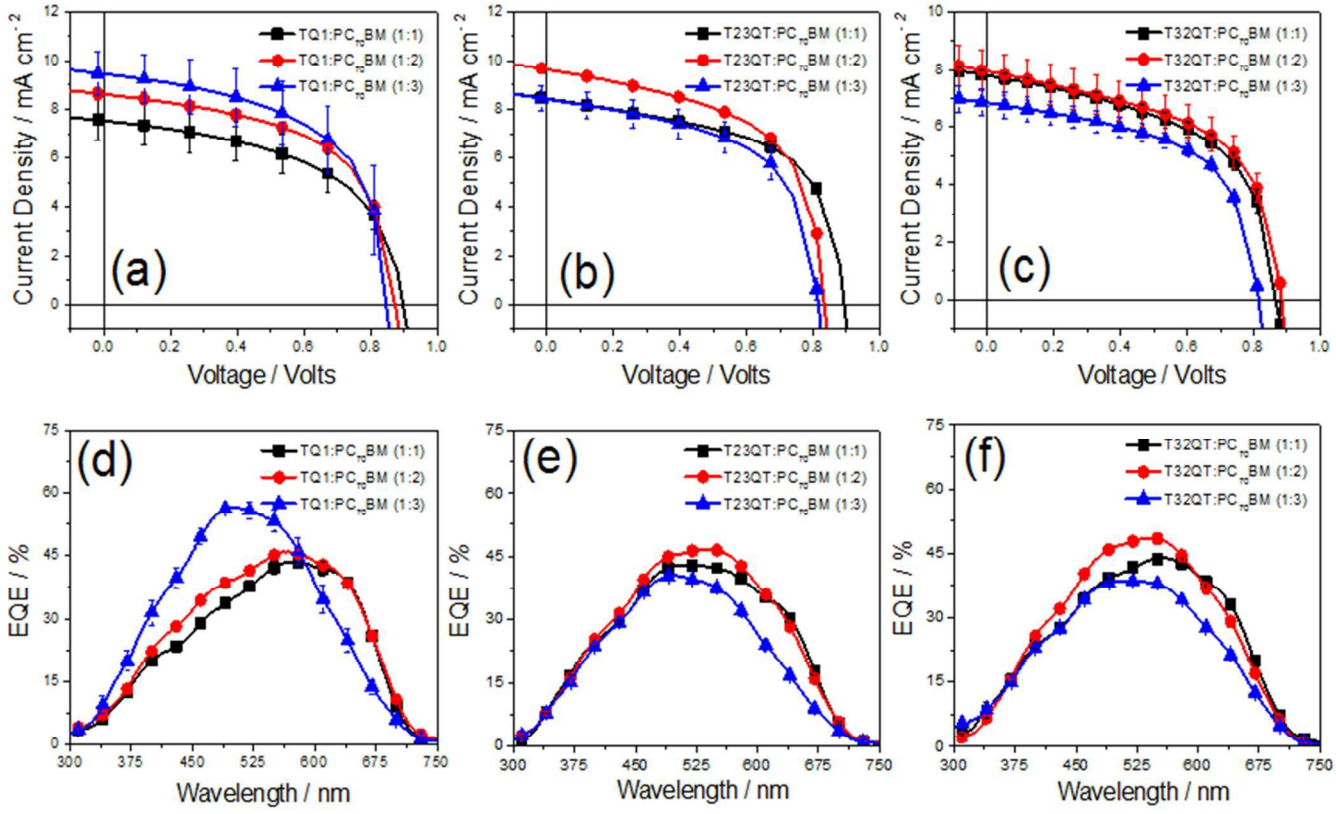

Table 3. The photovoltaic properties of the fabricated devices utilizing polymer:$PC_{70}BM$ photoactive layers in different composition ratio (1:1, 1:2 and 1:3) are presented.

Blend System	V_{oc} (Volts)	J_{sc} (mA/cm^2)	FF (%)	$(PCE)_{aver}$ (%)	$(PCE)_{max}$ (%)
TQ1:$PC_{70}BM$ (1:1)	0.89 ± 0.006	7.5 ± 0.32	54.3 ± 0.77	4.4 ± 0.22	4.6
TQ1:$PC_{70}BM$ (1:2)	0.88 ± 0.009	8.6 ± 0.19	57.0 ± 0.22	4.8 ± 0.14	4.9
TQ1:$PC_{70}BM$ (1:3)	0.84 ± 0.007	9.4 ± 1.45	59.6 ± 2.35	5.7 ± 1.07	6.6
T23TQ:$PC_{70}BM$ (1:1)	0.89 ± 0.01	8.5 ± 0.02	59.1 ± 1.89	4.9 ± 0.11	5.0
T23TQ:$PC_{70}BM$ (1:2)	0.83 ± 0.01	9.6 ± 0.02	57.3 ± 0.11	5.0 ± 0.13	5.0
T23TQ:$PC_{70}BM$ (1:3)	0.82 ± 0.01	8.5 ± 0.17	46.3 ± 1.13	3.4 ± 0.17	3.5
T32TQ:$PC_{70}BM$ (1:1)	0.87 ± 0.01	7.8 ± 0.06	55.5 ± 1.64	4.1 ± 0.17	4.3
T32TQ:$PC_{70}BM$ (1:2)	0.88 ± 0.01	8.1 ± 0.65	56.0 ± 0.34	4.7 ± 0.28	5.0
T32TQ:$PC_{70}BM$ (1:3)	0.82 ± 0.01	6.9 ± 0.58	48.3 ± 2.13	3.7 ± 0.42	4.0

Figure 7. Topography AFM images for (a) TQ1:$PC_{70}BM$ 1:3, (b) T23TQ:$PC_{70}BM$ 1:2 and (c) T32TQ:$PC_{70}BM$ 1:2. Scan scale 5 µm×5 µm